# Non-isothermal Soil Water Transport and Evaporation

**Jordi Grifoll and Josep Ma. Gastó**

Departament d'Enginyeria Química,
Escola Tècnica Superior d'Enginyeria Química
Universitat Rovira i Virgili, Catalunya, Spain
E-Mail: jgrifoll@etseq.urv.es

and

**Yoram Cohen**

Department of Chemical Engineering
and
Center for Environmental Risk Reduction
University of California, Los Angeles, Los Angeles, California 90095
E-Mail: yoram@ucla.edu

Submitted to

*Advances in Water Resources*

Submitted: October 20, 2004

Revised: July 10, 2006

## Abstract

A detailed model was formulated to describe the non-isothermal transport of water in the unsaturated soil zone. The model consists of the coupled equations of mass conservation for the liquid phase, gas phase and water vapor and the energy conservation equation. The water transport mechanisms considered are convection in the liquid phase, and convection, diffusion and dispersion of vapor in the gas phase. The boundary conditions at the soil-atmosphere interface include dynamical mass flux and energy flux that accounts for radiation transport. Comparison of numerical simulations results with published experimental data demonstrated that the present model is able to describe water and energy transport dynamics, including situations of low and moderate soil moisture contents. Analysis of field studies on soil drying suggests that that dispersion flux of the water vapor near the soil surface, which is seldom considered in soil drying models, can make a significant contribution to the total water flux.

**Keywords**: non-isothermal water transport; soil drying; soil moisture; soil temperature; evaporation; vapor dispersion; numerical simulation

## 1. - Introduction

The coupled transport of water liquid and vapor and energy in the unsaturated soil zone affects contaminant transport and volatilization [16], the efficiency of thermal remediation [14] and phytoremediation [56] of contaminated soils, nitrogen transformations and transport in the soil-plant system [20], the flux of $CO_2$ from a soil ecosystem that may affect global warming [55] and, air/soil fluxes of water and energy that impact continental weather [38]. Knowledge of energy and water transport in the soil is central to quantifying water resources in desert regions [67], design of underground electric power lines systems [1] and thermal energy storage in the unsaturated zone [52].

The pioneering work of Philip and de Vries [59], henceforth PDV, provided the first theory of non-isothermal moisture movement in porous materials. The PDV model consists of a water transport equation that considers both the vapor and liquid phases and an energy equation. This early model accounted for vapor phase diffusion with allowances for dependence of vapor pressure on temperature and matric potential (i.e., the Kelvin effect). Liquid transport included both gravity infiltration and transport associated with matric potential gradients due to both moisture content and temperature gradients. The energy equation considered conduction heat transfer and the latent heat of vaporization transported by the vapor. In order to account for local variations of temperature gradients in the air phase and for vapor flow through so-called liquid 'islands', the PDV model introduces enhancement factors for water vapor transport. Although it has been shown that the PDV model qualitatively describes the majority of earlier experimental data on non-isothermal water transport in porous media, in order to match experimental results with model predictions, empirical relations for water vapor enhancement factor have been proposed [15] to modify the original PDV model and utilized in numerical software

implementations of the model [69, 36]. However, such modifications have not yielded satisfactory agreement between PDV model predictions and field data [17, 11], while laboratory column studies have provided only limited support of the PDV theory [70]. Greater success was achieved with the modified PdV based water and heat transport model of Nassar and Horton [47] which was adapted to include osmotic pressure effects. A coupled water and heat transport model based on the PdV theory adapted to include osmotic pressure effects and interfaced with a solute transport model was developed by Nassar and Horton [47]. Experimental results for non-isothermal study in 10 cm-long soil columns [48] were reasonably consistent with the general trend of calculated water content and temperature profiles, specially for experiments in which wet conditions prevailed with initial volumetric water content equal or above 0.11 $m^3/m^3$. However, for initial conditions that represented relatively dry soil conditions predictions of soil moisture content exceeded measured value significantly near the hot end of the column.

Given the strong coupling of various mass and energy transport processes, various studies have attempted to assess the relative importance of various transport mechanisms of water transport under non-isothermal conditions[44, 45, 46, 5, 73]. Milly [45] utilized a modified PDV model[44], in which hysteresis in the soil/water retention curves was considered, to conclude that isothermal vapor diffusion flux (due to Kelvin effect) is higher than thermal vapor diffusion flux (due to vapor pressure dependence on temperature) of water transport near the soil surface. The above study illustrated that long time evaporation flux averages (1 month) are insensitive to considerations of non-isothermal effects. It is interesting to note that some experimental studies [46, 62, 63, 35] have suggested that, close to the surface, water liquid and water vapor fluxes are of the same order of magnitude. It is also interesting to note that

experimental studies [72, 11] have suggested that water vapor flux accounts approximately for half of the energy transport near the soil surface.

The impact of dynamic moisture changes near the soil surface on water evaporation from the soil has been the subject of a number of field studies [46, 5, 73]. For example, Monji et al. [46] observed that, over the period 8 a.m. - 12 a.m, the volumetric water content at the top 1 cm soil layer increased, while the evaporation flux also increased over the same period. The above result suggests that liquid water originating from the region below about 1 cm was the supply of water for both evaporation and liquid water storage near the top 1 cm soil region. Although moisture increase was attributed to liquid moisture movement due to temperature gradients, the PDV model formulation did not provide a quantitative explanation of such a behavior. In a later experimental study under arid conditions, Boulet et al. [5] reported the existence of a relatively dry soil layer, from surface to 25 cm depth through which water transport was mainly in vapor form, whereas water transport in liquid form dominated below this layer. In a later study, Yamanaka et al. [73] reported, based on field measurements and numerical simulations, the existence of an evaporation zone, at the bottom of a dry soil surface layer, which was thicker for fine-textured soils than for coarse-textured soils. The relative roles of vapor and liquid fluxes on water transport from the inner soil to the soil/atmosphere interface was explored by Saravanapavan and Salvucci, [66] using a numerical PDV model. Their results indicate that, while vapor diffusion dominates total moisture transport near the soil surface, liquid transport controls evaporation at daily time scales in the deeper layers of the soil for all but very dry soils.

Significant discrepancies were noted by Cahill and Parlenge [11] when comparing measured vapor fluxes with those estimated from the PDV theory. These authors concluded that the PDV theory is incomplete with respect to the description of vapor transport. Parlange et al,

[57] suggested that contraction and expansion of air near the soil surface could transport water vapor by convection. They argued that the omission of such a mechanism from the PDV theory could explain the deviation of the PDV calculations of [11] from their measured vapor fluxes. In a later study, Or and Wraith [54] questioned the above measurements, claiming that moisture content as determined by time domain reflectometry should consider the important temperature effects on soil bulk dielectric permitivity. It is that the prevailing opinion regarding non-isothermal water transport in soil [11] that although the PDV theory is the basis for most soil-atmosphere continuum models in use today, there has not been a satisfactory comparison of water vapor flux measured in field soils with a theory for moderate soil moisture contents.

In this study, we present a general model formulation of water and energy transport in unsaturated porous media. In addition to the mechanisms considered by PDV, the present model accounts for convective transport in both the gas and liquid water phases in addition to vapor dispersion and liquid sensible heat dispersion, without introducing empirical vapor-transport enhancement factors as is done in the PDV type models. Convection in the gas phase was considered due both to variations in liquid content and gas density temperature effects. At the soil/atmosphere boundary energy and mass transport flux conditions are considered. The present analysis is restricted to constant atmospheric pressure whereby potential effects due to atmospheric pressure changes are not considered. Results from numerical simulations with the present model are presented to elucidate the significance of the various water transport mechanism and provide the basis for analyzing non-isothermal diurnal cycles of moisture content and temperature profiles from field soils. Model results are also compared with classical experimental studies on water transport in soil [35, 62].

## 2. Model description

### 2.1 Mass balance equations

The unsaturated soil domain consists of soil-solids, liquid water and a gas phase composed of air and water vapor. The present approach to modeling water transport in the soil domain considers transport equations for liquid water, gas phase and the water vapor.

The liquid water mass balance is expressed as [3]:

$$\frac{\partial \theta_L \rho_L}{\partial t} = -\nabla(\rho_L \mathbf{q_L}) - f_{LG} \tag{1}$$

where $\rho_L$ (kg/m$^3$) is the liquid water density, $\theta_L$ (m$^3$/m$^3$) is the volumetric liquid water content, $\mathbf{q_L}$ (m/s) is the liquid phase flux or specific discharge, $f_{LG}$ (kg/m$^3$ s) is the phase change water flux, that results in water transfer from the liquid to the gas phase, per unit volume of porous soil matrix, and $t$ (s) is time. The liquid phase flux is expressed by the extension of Darcy's law [18, 30]

$$\mathbf{q_L} = -\frac{k_i k_r}{\mu_L}(\nabla P_L - \rho_L \mathbf{g}) \tag{2}$$

where $k_i$ (m$^2$) is the intrinsic permeability, $k_r$ (dimensionless) is the relative permeability, $\mu_L$ (kg/m s) is dynamic water viscosity, $\mathbf{g}$ (m/s$^2$) is the gravitational acceleration vector and $P_L$ (Pa) is the matric pressure (pressure difference between the liquid and gas phases). In these equations $\mu_L$ and $\rho_L$ are considered to be temperature dependent (see Table 1).

The liquid content $\theta_L$ and the matric pressure $P_L$ can be related via a so-called soil-characteristic curve which is usually reported in most studies at a temperature of 20°C. The dependence of the soil water characteristic curve on temperature was described following the

approach of Liu and Dane [40]. In this approach, the total volumetric water content, $\theta_L(T)$, is considered to be the result of contributions of continuous and funicular water regions, the latter being dependent on the reference volumetric water content (temperature dependent), the saturation (temperature independent) and the residual (temperature dependent) volumetric water contents ($\theta_L(T_0)$, $\theta_{LS}$ and $\theta_{LR}(T)$, respectively). This temperature-dependent volumetric content can be expressed as [40]

$$\theta_L(T) = \theta_L(T_0) - \frac{\theta_{LS} - \theta_L(T_0)}{\theta_{LS} - \theta_{LR}(T_0)}\left[\theta_{LR}(T_0) - \theta_{LR}(T)\right] \tag{3}$$

in which $T$ is temperature and $\theta_{LR}(T_0)$ is the residual volumetric content at the reference temperature $T_0$. It is noted that $\theta_L(T)$, and $\theta_L(T_0)$ would correspond to the same matric pressure if surface tension dependence on temperature is neglected. However, it is well accepted that, for given continuous water content, the matric pressure will be impacted by the variation of surface tension with temperature as given by the following relation [e.g. 44]

$$P_L(T) = P_L(T_0)\frac{\sigma(T)}{\sigma(T_0)} \tag{4}$$

where $\sigma(T)$ (N/m) is surface tension, which is calculated as a function of temperature as given in Table 1. Therefore, as implied by Eqs. (3) and (4) water saturation at a given temperature has a correspondingly unique matric pressure. Finally, we note that based on experimental data from several sources [28, 31, 32, 68] it can be shown that the dependence of $\theta_{LR}$ on temperature follows the following simple linear relationship as suggested by She and Sleep [68]

$$\frac{\theta_{LR}(T)}{\theta_{LR}(293\ K)} = 1 - a(T - 293\ K) \tag{5}$$

in which $a$ is an empirical constant that can vary with the specific soil under consideration. Analysis of data for three soils [28, 31, 68] revealed a weak dependence of $a$ (0.004 ± 0.002) on soil type.

The mass balance equation for the gas phase as a whole (dry air and water vapor) is [3]

$$\frac{\partial \theta_G \rho_G}{\partial t} = -\nabla(\rho_G \mathbf{q_G}) + f_{LG} \tag{6}$$

where $\theta_G$ ($m^3/m^3$) is gas phase volumetric content (where the soil porosity is given as $\phi = \theta_L + \theta_G$) and $\rho_G$ ($kg/m^3$) the density of the gas phase. Throughout the system domain, the total gas phase pressure was taken as atmospheric. However, it is noted that gas density can vary due to changes in water vapor concentration and temperature. Also, in the present model, gas phase movement is primarily due to liquid content variation, and gas expansion or contraction due to temperature changes.

The mass balance equation for vapor water can be expressed as [3]:

$$\frac{\partial \theta_G \rho_v}{\partial t} = -\nabla \cdot (\rho_v \mathbf{q_G} + \theta_G \mathbf{J_{hG}}) + f_{LG} \tag{7}$$

where $\rho_v$ ($kg/m^3$) is the water vapor density, $\mathbf{q_G}$ (m/s) is the gas phase flux and $\mathbf{J_{hG}}$ ($kg/m^2s$) is the hydrodynamic dispersion flux expressed as [3]:

$$\mathbf{J_{hG}} = -\left(\frac{D_G}{\tau_G} + \mathbf{D}^M_{m\mathbf{G}}\right) \cdot \nabla \rho_v \tag{8}$$

In which $D_G$ ($m^2/s$) is the diffusion coefficient for water vapor in air (Table 1) and $\mathbf{D}^M_{m\mathbf{G}}$ ($kg/m^2$) is the tensor of mechanical dispersion, which is related to the porous medium's dipersivities [3]. The water vapor tortuosity, $\tau_G$ (dimensionless), was evaluated in the present model simulations

according to the first model of Millington and Quirk, [42,43], i.e. $\tau_G = \phi^{2/3}/\theta_G$, as suggested by Jin and Jury [37].

The liquid and vapor water in the soil matrix were considered to be in local equilibrium. The water vapor density (or mass concentration) was calculated from the water vapor pressure, $P^*$ (Pa), assuming ideal gas behavior and correcting for the curvature effect of the gas/liquid interface, as stated by Kelvin's equation [3]

$$\rho_v = \frac{P^* M}{R\ T} \exp\ \left( \frac{P_L\ \ M}{\rho_L\ \ R\ \ T} \right) \tag{9}$$

where $M$ (kg/mol) is the molecular mass of water and $R$ (J/K mol) is the universal gas constant.

### 2.2 Energy balance equation

In the present model formulation, local thermal equilibrium is assumed which implies that within a representative elementary volume the temperature of all phases that compose the porous media is the same [3]. It is noted that an order of magnitude analysis by Milly [44] suggests that the thermal equilibrium assumption may be violated only at relatively high mass fluxes in coarse soils.

The energy balance over a representative elementary control volume can be expressed as [3]:

$$\frac{\partial \left[ \theta_L \rho_L u_L + \theta_G \rho_G u_G + (1-\phi) \rho_S u_S \right]}{\partial\ t} + \nabla \mathbf{Q} = 0 \tag{10}$$

where $u_L$, $u_G$, $u_S$ (kJ/kg) are the specific internal energies corresponding to the liquid, gas and solid phases, respectively, and $\mathbf{Q}$ (kJ/m$^2$ s) is the total energy flux due to convection of the liquid

and gas phases, water vapor dispersion, conduction and thermal dispersion in the liquid phase. It is reasonable to assume that thermal dispersion in the gas phase should be negligible when compared to the thermal dispersion in the liquid phase [3]. Accordingly, the total energy flux is given by

$$\mathbf{Q}=\rho_L q_L h_L+\rho_G q_G h_G+\theta_G J_{hG}(u_v-u_a)-\left(\lambda_{eff}+\theta_L \rho_L C_{vL}\mathbf{D}_{\mathbf{mL}}^{\mathbf{H}}\right)\nabla T \tag{11}$$

where $h_L$ and $h_G$ (kJ/kg) are the specific enthalpies for the liquid and gas phases, respectively, $u_v$ and $u_a$ (kJ/kg) are the specific internal energies corresponding to the water vapor and dry air, respectively, $C_{vL}$ (kJ/kg J) is the liquid phase specific heat capacity and $\mathbf{D}_{\mathbf{mL}}^{\mathbf{H}}$ is the mechanical thermal dispersion tensor. Finally, the effective soil thermal conductivity, $\lambda_{eff}$ (kW/m K), can be estimated following the correlation of Campbell [13].

$$\lambda_{eff} = A + B\theta_L - (A - D)\exp\left[-(C\theta_L)^E\right] \tag{12}$$

where $A$, $B$, $C$, $D$ and $E$ are soil dependent empirical coefficients that can be estimated from soil bulk density, soil porosity and the clay fraction.

### 2.3 Simulation set up, dispersivities and boundary conditions

The most relevant variations of moisture and temperature in the soil domain typically take place in the vertical direction and near the surface region. In fact, the most detailed experimental studies have focused on measurements of vertical temperature and moisture profiles. Therefore, in the present study, we focus on one-dimensional transport simulations for comparison with available experimental results.

Solution of the mass and energy equations requires specification of the mass and energy mechanical dispersion tensor which reduces to a longitudinal dispersion coefficient for one-dimensional transport. For the liquid and gas phases, the longitudinal dispersion coefficient, $D_{l\,i}^{j}$, where $i$ = L, G (liquid or gas) and $j$ = M, H (mass or heat), can be expressed as a function of the pore-fluid velocity [3]

$$D_{l\,i}^{j} = \alpha_{l\,i}^{j}\, v_i \tag{13}$$

where $\alpha_{l\,i}^{j}$(m) is the longitudinal dispersivity and the pore fluid velocity in phase $i$ is given as $v_i = q_i / \theta_i$. . It is noted that theoretical studies [3] have suggested that it is reasonable to employ the analogy between thermal and chemical mass transport dispersivities. Experimental data available for dispersion in granular packed beds [26] confirms that well below the transition to turbulent flow (as it is the case in the present study) the behavior of dispersion is the same for both gases and liquids. It has been argued that in theory, it is plausible that under two phase flow conditions, the dispersivity for wetting and non-wetting phases may differ somewhat [65] due to pore geometry and connectivity effects. In the present study, however, given the lack of experimental data for the range of saturations of interest, we adopt the approach taken in previous studies [71,25] utilizing a first order approach in which the local dispersivities are taken to be functions of the local phase saturation. Accordingly, based on analysis of available experimental data [41, 27, 53] and numerical model estimates [65], the following correlation was developed [21]

$$\frac{\alpha_{li}^{j}}{\alpha_{li}^{j0}} = 13.6 - 16\, S_i + 3.4\,(S_i)^5 \tag{14}$$

in which $S_i = \theta_i / \phi$ is the phase $i$ saturation and $\alpha_{li}^{j0}$ is the phase $i$ dispersivity at saturation. We

note that, given the general lack of dispersivity values for the specific soils in the present test cases, the saturation dispersivity used in the above correlation was taken to be 0.078 m, as reported in the field experiments of Biggar and Nielsen [4] and shown to be a reasonable value in previous modeling studies [16, 25].

The boundary conditions at the bottom of the system domain for equations (1), (6) and (10) were set as $\partial P_L/\partial z = 0$, $\partial \rho_v/\partial z = 0$ and $\partial T/\partial z = 0$, and, for equation (9), $q_G = 0$. At the soil surface the evaporation flux is set as

$$J_{w0} = k_{atm} \left( \rho_{v\_atm} - \rho_v \big|_{z=0} \right) \tag{15}$$

in which $k_{\text{atm}}$ (m/s) is the atmospheric-side mass transfer coefficient and $\rho_{v\_atm}$ and $\rho_v \big|_{z=0}$ are the water vapor mass concentration in the atmosphere and at the soil interface, respectively. We note that $\rho_v \big|_{z=0}$ is calculated from the matric pressure and temperature at the soil surface using equation (9). In the current model comparison with field data, due to lack of atmospheric stability data for the field studies, the mass transfer coefficient, $k_{\text{atm}}$, was calculated assuming neutral stable atmosphere [9, 24].

The top boundary condition for the energy equation, which accounts for the different energy forms that reach the soil surface, is given as

$$R_n + q_0 + J_{w0} h_v = Q_0 \tag{16}$$

where $R_n$ (W/m$^2$) is the net radiation flux, $q_0$ (W/m$^2$) and $J_{w0}\ h_v$ (W/m$^2$) represent the surface sensible heat and latent heat fluxes, respectively, and $Q_0$ (W/m$^2$) is the total energy flux to the soil as given by Eq. (11). The net radiation flux, $R_n$, includes short-wave flux as a function of geographical longitude and latitude as well as day of year, local time, atmospheric absorption

and dispersion, and fraction of cloud cover in the sky [6]. In the present simulations, clear skies were assumed when information about cloud coverage was unavailable. The albedo was considered to depend on moisture content at the soil surface according to the relationship given by Idso et al. [33]. Longwave radiation flux from the atmosphere was computed using the emissivity values given by Idso [34] as a function of water vapor pressure and surface air temperature. Given that most natural surfaces have emissivities greater than 0.95 [6], longwave emission from the soil surface was computed assuming the surface to be a black body.

Sensible heat flux from the soil surface to the atmosphere was estimated as

$$q_0 = h_{atm}\left(T_a - T\big|_{z=0}\right) \tag{17}$$

where $h_{atm}$ (W/m$^2$ °C) is the soil surface/atmosphere heat transfer coefficient, $T_a$ (°C) is the air temperature and $T\big|_{z=0}$ (°C) the temperature at the soil surface. Both the heat (Eq 17) and mass (Eq 15) transfer coefficients were estimated from the model of Brutsaert [9] as adapted by Grifoll and Cohen [24] given meteorological data (temperature and wind speed), surface characteristics (surface roughness) and physicochemical properties (air viscosity and density and water vapor thermal and vapor diffusivities).

It is important to recognize that the soil surface boundary conditions for sensible heat transfer (Eq. 17) and evaporation (Eq. 15) are affected by diurnal cycling of air temperature ($T_a$) and relative humidity ($H$) at the upper edge of the dynamic sublayer of the atmosphere at a reference height, taken as 2 m in this study. These diurnal cycles can be described by the following well-established empirical relations [45]

$$T_a = \overline{T_a} + A_T \sin\left[\frac{\pi}{12}\left(t_h - \varphi_T\right)\right] \tag{18.a}$$

$$H = \overline{H} - A_H \ \sin\left[\frac{\pi}{12}\left(t_h - \varphi_H\right)\right] \tag{18.b}$$

where $\overline{T_a}$ and $\overline{H}$ represent daily average temperature and relative humidity, respectively, $A_T$ and $A_H$ are the oscillation amplitudes, $\varphi_T$ and $\varphi_H$ are the time phase lags between $T_a$ and $H$ maxima and midnight, and $t_h$ is the time in hours from midnight.

**2.4 Numerical solution scheme**

The one-dimensional transport equations for liquid water, gas, vapor water, and energy, (Eqs. 1, 6, 7 and 10) were solved by a fully implicit finite-volume approach [58,23]. Second derivatives (flux terms) were discretized using a central differencing scheme and the time derivative were approximated by backward differencing [19].

The discretized mass and energy transport equations were solved using a triple iterative scheme for each time step as shown in figure 1. The $P_L$, $f_{LG}$ and $T$ profiles at time t were initially guessed for the time step $t + \Delta t$ . The equations for liquid water movement (Eqs.1 and 2) are then solved by a Newton-Raphson iteration procedure [61, 23] with a convergence criterion set to be when the liquid water mass balance in each cell is attained at a discrepancy below the given tolerance of one millionth of the residual water content. Subsequently, the gas transport equation (6) is solved to obtain the $q_G$ profiles, followed by a solution of equation (7) to obtain the profiles of $f_{LG}$. The $f_{LG}$. profiles are then compared with the previously assumed $f_{LG}$ values and the iterative procedure repeats (using the last computed values as the initial guess) if at any point the discrepancies between the guessed and computed profiles are higher than 0.01%. When convergence is reached, the energy balance, equation (10), is solved and the calculated

temperature profile is compared to the guessed profile. If differences between the calculated and the guessed profile are higher than 0.001ºC the procedure restarts until global convergence is attained for all grid point temperatures at $t + \Delta t$ .

The total soil depth of the simulation domain was set equal to 2 m and was divided into three zones. The top zone ($0 < z < 0.08$ m) was divided into step sizes of 0.001 m. In the second zone below ($0.08 \text{ m} < z < 0.6714$ m) the step size was increased progressively from 0.001 m to 0.05 m such that $\Delta z_i = r \cdot \Delta z_{i-1}$ with $r = 1.1$. The step size in the final zone ($0.6714 < z < 2.0214$ m) was set to 0.05 m. A variable time step was selected in the range of 0.5-3600 s, to maintain the number of outer iterations (converge of temperature) $\leq 8$. If convergence was not attained after the eighth iteration, the time step was reduced by 10% and the calculation procedure for this time step was restarted. On the other hand, if less than four global iterations were needed the subsequent time step was increased by 10%. When solving transport equations (1) and (10), the local grid compliance of the Courant and Péclet number restrictions was maintained ($v_{eff}\ \Delta t / \Delta z << 1,\ \Delta z\ v_{eff} / D_{eff} << 2$). Grid independence of the solution was determined, for all test cases, by carrying out simulations for grid sizes that were progressively decreased (by 50% for each successive simulation) until the maximum difference in volumetric water content, (along the depth of the soil column), with respect the preceding simulation, was less than 0.1%.

The numerical algorithm for the solution of the liquid water content (Eq. 1) was checked by comparing simulation results against previously published numerical results for water transport in a loam-type soil [25] and with the analytical solution of water infiltration of Broadbridge and White [7]. The numerical algorithm for the energy transport was checked against the analytical solution of the one-dimensional conductive heat transport equation with a sinusoidal temperature

variation set as a top boundary condition. In all cases, the present algorithms performed with deviations below 0.01% with respect to the local volumetric water content or temperature.

## 3. Results and discussion

### 3.1 Test case I

The first test case was based on the experimental field study of Rose [62]. In this experimental study, a bare homogeneous loamy sandy soil plot (located in Alice Springs, Australia) was irrigated, and the depth profiles of water content and temperature were monitored in the top 15 cm soil region for a period of 6 days and nights. Temperature-time profiles were reported only for the soil surface and at depth of 13 cm. Information regarding the precise dates during which the experimental study was carried was not reported; however, in a private communication C. W. Rose has informed the authors that his study [62] was carried out during the month of September. The average temperature and wind speed for the month of September were obtained from the Australian Data Archive for Meteorology [2] with the relevant climatological and geographical data provided in Table 3.

In the Rose [62] experiments, for the first six days after irrigation core soil samples of ½ or 1” thickness were taken at three locations (0-½”, 1-1½” and 5-6”) and moisture content for the different core samples were determined by gravimetry. In day four, moisture measurements were reported for a more refined profile over a depth of 13 cm. Since the study plot was homogeneous soil, the hydraulic characteristics were depth invariant and these were fitted using the Brooks and Corey [8] equations

$$\theta_L = \theta_{LS}\left(\frac{P_b}{P_L}\right)^{\lambda} \quad \text{if } P_L < P_b$$
$$\theta_L = \theta_{LS} \quad \text{if } P_L \geq P_b \tag{19}$$

and

$$k_r = \left(\frac{P_b}{P_L}\right)^{2+3\lambda} \quad if\ P_L < P_b$$
$$k_r = 1 \quad if\ P_L \geq P_b \tag{20}$$

In which $P_b$ and $\lambda$ are model parameters, given in Table 2. We also note that for the model simulations, the initial temperature and $\theta_L$ soil profile was based on a fitted spline function that encompasses the reported initial profiles for the top 13 cm [62] and assuming uniform values for the region below.

It should be noted that the moisture contents reported in the Rose [62] study represent average values (along the depth location) for each of the core samples. Accordingly, the simulation results for moisture content were integral averaged over a depth corresponding to the thickness of the specific core samples. A comparison of the experimental and simulation average moisture content results for days 1-6 after irrigation is provided in Figure 2 for the three specific core samples (0-1.27 cm, 2.54-3.81 cm and 12.7-15.2 cm) along with the moisture content at the lower and upper boundaries of the core samples. The general trend of the simulation results closely follows the measured values, suggesting that the model captures the essential processes that govern non-isothermal moisture transport in the soil. Diurnal cycling of moisture content are apparent as one moves below the surface but decays rapidly as a depth of about 2.5 cm is approached. The moisture content gradients are most pronounced near the soil surface which is indicated by the difference between the moisture contents at z = 0 and z = 1.27 cm, about 0.1

$m^3/m^3$ in day one, but it decreases with time. In this surface region water evaporation and water vapor transport are responsible for the rapid decline in moisture content as the surface is approached. It is noted that, at depth below 12.7 cm the experimental data scatter overshadows any diurnal moisture cycling which, based on the simulations, is in itself negligible. The quantitative agreement of the simulation results with the data is reasonable over the soil depth locations, with the highest deviations in the surface region (0-1.27 cm) in which the average and maximum discrepancies between the measured and simulated moisture content are 27.5 and 55.9 %, respectively, with the maximum deviation corresponding to 3.2 days after irrigation. Such a discrepancy level was reported in other studies, specially under low moisture and high temperature conditions. For example, the PDV based model of Nassar et al. [49] led to about 33% higher prediction of soil moisture content when compared with experimental results near the drier surface ($\theta_L$ ~ 0.18) of a silty clay loam soil column [50]. In another related experimental study with a laboratory soil columns [51], measured water contents near the hot end ($\theta_L$ ~ 0.08) were about 37% higher than predicted with a PDV model when the mean temperature of the soil was 50°C. It is noted that closer agreement of predicted and measured values was obtained in similar experiments [51] with mean soil temperatures of 10°C and 27°C.

The diurnal temperature profiles for the two depths (surface and 13 cm) reported in the study of Rose [62] were reasonably predicted by the model simulations as shown in Figure 3. The diurnal temperature cycles which are expected due to the daily radiation cycle, are clearly predicted in the simulation. The average discrepancy between the model predictions and the data, over the course of the field study, is 6.6°C with the maximum deviation of 26°C at approximately 5:30 p.m. in the fifth day. For the first four days, the maxima in the surface diurnal temperature is predicted to occur at 1 p.m. relative to about 2 p.m. according to the

reported data. In the fifth day, however, the predicted occurrence of the maximum temperature (0:46 p.m.) deviates more substantially from the reported data (5:30 p.m). Such deviation could be due to differences in local meteorological conditions, which were not reported in the study of Rose [62], compared to the use of typical conditions used in the simulations for the month of September. It is also noted that there is a lag time of approximately 1.5 hours between the measured and calculated temperature cycle at the soil surface. This time lag could be, in part, due to uncertainties in the measured surface temperature given the steep temperature gradients in the surface region..

A comparison of predicted and field measured temperature and water vapor partial pressure profiles reported by Rose [62], at 4 a.m. and 2 p.m. for the fifth day after irrigation, is provided in Figure 4, along with additional simulation profiles for 9 a.m. and 7 p.m. Clearly, the predictions closely follow the reported experimental data for both temperature and water vapor partial pressure. The maximum deviations between the predictions and field data, for temperature and water vapor partial pressure, are 14% (4ºC) at 2 p.m. at a depth of 13 cm and 40% (46 mm Hg) at a depth of 9 mm. It is noted that both the predicted and experimental vapor partial pressure profiles display a change of slope near the surface which marks the location of maximum evaporation flux. The presence of this vapor partial pressure maximum is a typical feature of drying soils that has been reported and analyzed in previous experimental studies [e.g. 5, 73]. Above this depth (towards the surface), water vapor transport is the dominant mechanism of water transport, whereas liquid water migration is the main water transport pathway below this depth.

### 3.2 Test case II

The second test case is based on the experimental study of Jackson [35] on moisture transport in an Adelanto loam soil in Phoenix (Arizona). In that study the soil was irrigated with 10 cm of water on March 2, 1971 and the evolution of the average moisture content in the top 0.5 cm of the soil was monitored for a period of three days (on March 7, 8 and 9). The reported volumetric water content–matric pressure data could not be adequately fitted by the Brooks and Corey and the van Genuchten type functions. However, a good data fit was obtained for the above data using the Haverkamp et al. [29] type of function

$$\theta_L = \frac{\theta_{LS} - \theta_{LR}}{1 + \left(P_L / \alpha\right)^{\beta}} + \theta_{LR} \qquad (21)$$

where the fitting parameters ($\theta_{LS}$, $\theta_{LR}$, $\alpha$, $\beta$) for this soil are given in Table 2. Data for soil relative permeability, which varied with matric pressure [35], were fitted to a Brooks and Corey [8] type of hydraulic function (Eq. 20). Mixing the Haverkamp and Brooks and Corey hydraulic functions should be viewed here as merely an empirical approach for the purpose of data fitting and interpolation. Since the prevailing wind speed, atmospheric relative humidity and temperature were not reported for the Jackson [35] study, these meteorological parameters were approximated by the average values given by Ruffner and Bair [64], for Phoenix at the month of March. These data were then fitted to the daily cyclic functions as given in equations (18 a,b) with the fitting parameters reported in Table 2. The initial volumetric water content profile used in the simulations was set based on the reported experimental values at 0:0 a.m. of day 5 after irrigation (March 7) just at the beginning of the data collection period. However, since soil temperature profiles were not reported, a reasonable initial temperature profile was set by first solving the coupled mass and energy equations (1, 10) with the initial conditions of a saturated

soil at a uniform temperature of 15ºC. The temperature profile at the end of a four days simulation was then taken as the initial condition for the test case.

The predicted average moisture content values at different depths (0-0.5 cm) (Figure 5) clearly depict the decaying diurnal temporal cyclic moisture profiles. The predicted volumetric water content, $\theta_L$, at the surface and at depths of 0.2, 0.3 and 0.5 cm, reveal moisture gradients that increase near the soil surface with the maximum gradients occurring at ~ 0:30 p.m. Although the predicted average moisture content for the top region (0-0.5 cm) tracks the reported experimental moisture content, we note that the peak moisture contents at ~ 7 a.m. of days 6 and 7 were underpredicted by 25% and 32%, respectively. These differences were similar to the deviations found in Test Case I. It is plausible that such differences are, in part, due to the use of average monthly meteorological data instead of the lacking actual conditions for the specific dates in which the experiments were conducted. In order to assess the impact of meteorological conditions on the evolution of the average soil moisture profile (for the region 0-0.5 cm) a series of simulations were carried out. A sensitivity study was conducted for wind speeds of 2, 3 and 4 m/s at $\overline{H}$ = 0.40 and for $\overline{H}$ = 0.60 at speed of 3 m/s. As revealed by the simulation results, the moisture content decreased (in the surface region of 0-0.5 cm) with increasing wind speed (Figure 6), reflecting the fact that water transport limitation within the porous matric become more pronounced with increasing evaporation rate (as wind speed is increased). The impact of wind speed diminishes progressively with time as the soil dries. The predicted moisture content also increases, as expected, with increasing relative humidity owing to the decrease of evaporation flux with relative humidity. We note that upon increasing the relative humidity from 0.4 to 0.6, the simulated moisture content approaches the experimental results. The above sensitivity analysis clearly suggests that in order to fully interpret results from field studies of

non-isothermal water transport in soil, it is imperative that such studies provide detailed (hourly) reporting of meteorological data for the periods of time for which the studies are conducted.

Insight into the relative importance of the various transport mechanism that affect the total water flux, can be gained by inspecting the water flux depth profiles associated with transport due to convection, diffusion and dispersion. As an illustration, the water flux simulation profiles are shown in Figure 7 for day 7 at 2 p.m. for the Jackson experiment (Test Case II). For the specific condition of Figure 7, the moisture content near the surface was lowest over the experimental monitoring period, thus enabling an assessment of the role of vapor transport in the top surface region. In the region between 0.5 and 2 m, in which volumetric water content and temperature variations are nearly uniform (with variations of at most 0.15% and 0.3ºC, respectively) liquid transport is primarily due to gravity flow. Clearly, in the absence of moisture gradients, all gradient driven mechanisms (diffusion and dispersion) are absent. As one moves up from a depth of 0.5 to 0.01 m, the volumetric water content decreases (from a value of 0.27 at 0.5 m) by about 50%. The moisture gradient in this region is sufficient to overcome gravity and induces a convective transport of liquid water towards the surface. This resulting convective flux increases until it reaches a maximum at a depth of about 0.01 m. Above this depth, convective liquid water flux diminishes rapidly as the volumetric water content, in the surface region (0.006-0 m) drops below about 0.06 $m^3/m^3$. About 73% of the water flux to the atmosphere is made up by the upward convective flux of liquid water that reaches the depth of 0.01 m from below, while the remaining 27% is from the evaporation at the boundary of the soil wet region, near the surface. This example illustrates that water evaporation is controlled by liquid convection below the dry zone (below depth of about 0.01 m in this example), as also supported by the study of Saravanapavan and Salvucci [66]. Below the dry zone, there is a wet region (0.5-0.01 m) in which temperature increases from 15.5ºC to 40.4ºC inducing a progressive increase of water vapor concentration with depth, which in turn results in a downward water vapor diffusive flux. This downward vapor diffusion flux is relatively low when compared with the upward liquid

convection with a maximum ratio of vapor diffusion to liquid convection flux of 0.059 reached at z ~ 0.015 m.

In the very top surface region, extending from depth of 0.01 m to the surface, there is a dramatic change in the contribution of the various transport mechanisms to the net water flux. Liquid water content in this zone is extremely low ($0.03 \leq \theta_L \leq 0.12$) such that liquid water convection is negligible and water transport is dominated by the gas phase. Vapor convection in this gas phase is not a very active mechanism, for example the contribution of vapor convection to the total upward water flux in this region is minimal and reaches a maximum of about 3.7% . Similar or lower contributions of vapor phase transport by convection to the total water flux were also observed for the simulation pertaining to the Rose study (i.e., Test Case I). The above results suggest that, under constant atmospheric pressure condition, vapor convection is not a dominant mechanism for water vapor transport near the surface.

As the illustration of Fig. 7 reveals, in the top soil zone water vapor flux is primarily due to diffusion (~ 60% of the total flux) with water vapor dispersion in the gas phase accounting for about 40% of the net water flux in the immediate surface region 0.005-0 m. It is important to recognize that, although dispersion is an outcome of convection, even in this relatively dry surface zone, in which convective transport is limited, vapor transport due to dispersion is significant. The above seemingly, unexpected behavior is the result of the extraordinary high vapor concentration gradients that occur in the dry layer of the near surface region.

The early PdV based modeling studies recognized that water vapor flow in porous media, in the presence of temperature gradients, could not be adequately described by considering only vapor flux by diffusion. In order to match experiments with theoretical predictions of the PdV approach, the enhancement factor was introduced to account for local variations of temperature

gradient and vapor flow trough so-called liquid 'islands'. The present work suggests that that dispersion should also be considered as a contribution to this 'enhanced' flux. Water vapor is a component of the soil gas phase that disperses via the gas phase in the porous soil matrix when water vapor concentration gradients exists in the soil. Clearly, experimental investigation is warranted to evaluate the importance of water vapor dispersion under non-isothermal and isothermal conditions to water transport in the soil environment.

## 4. Conclusions

A model formulation for coupled transport of liquid and vapor water and energy in unsaturated porous media has been presented to describe non-isothermal water transport in the soil vadose zone. This non-isothermal model includes interphase water transport between the gas and liquid phases, convection, diffusion and dispersion of water vapor, convection of liquid water and convection, conduction and dispersion for the energy transport. Comparison of model simulations, for the condition of constant atmospheric pressure, with classical field evaporation experiments demonstrated that the model describes the time evolution of volumetric water content, water vapor partial pressure and temperature to a reasonable accuracy indicating that the model formulation captures the essentials of the involved transport processes. Detailed analysis of the various transport mechanisms indicates that when evaporation leads to the occurrence of a near-surface dry soil layer (stage-two evaporation), diffusion and dispersion of water vapor are the significant water transport mechanisms in the upper layer of the soil where low liquid water content impedes liquid water migration. It is noted that in this upper soil layer dispersion transport of water vapor could be relevant (up to 35% of the total water flux) even when the contribution of gas-phase convection to the overall water transport is relatively small.

## Acknowledgments

The financial assistance received from the DGIN of Spain, project PPQ2001-1519 is gratefully acknowledged. Partial support was also received from the UCLA Center for Environmental Risk Reduction.

## References

[1] Anders GJ, Radhakrishna H. Power cable thermal analysis with consideration of heat and moisture transfer in the soil. IEEE Trans Power Deliv 1988; 3:1280–1288.

[2] Australian Data Archive for Meteorology (ADAM). Australian Bureau of Meteorology (http://www.bom.gov.au/climate/averages/tables/cw_015540.shtml) 2003.

[3] Bear J, Bachmat Y. Introduction to Modeling of Transport Phenomena in Porous Media. Dordrecht: Kluwer, 1991.

[4] Biggar JW, Nielsen DR. Spatial variability of the leaching characteristics of a field soil. Water Resour Res 1976; 1: 78-84.

[5] Boulet G, Braud I, Vauclin M. Study of the mechanisms of evaporation under arid conditions using a detailed model of the soil-atmosphere continuum. Application to the EFEDA and experiment, J Hydrol 1997; 193: 114-141.

[6] Bras RL. Hydrology. Reading: Addison-Wesley, 1990.

[7] Broadbridge P, White I. Constant rate infiltration. A versatile nonlinear model, 1. Analytic solution. Water Resour Res 1988; 24(1): 145-154.

[8] Brooks RH, Corey AT. Hydraulic properties of porous media, Hydrol. Pap. 3, Colorado State University, Ft. Collins, 1964.

[9] Brutsaert W. A theory for local evaporation (or heat transfer) from rough and smooth surfaces at ground level. Water Resour Res 1975; 4: 543-550.

[10] Brutsaert W. Evaporation into the atmosphere. Norwell: Kluwer, 1982.

[11] Cahill AT, Parlange MB. On water vapor transport in field soils. Water Resour Res 1998; 34(4): 731-739.

[12] Cahill AT, Parlange MB. Reply. Water Resour Res. 2000; 36(10): 3107-3110.

[13] Campbell GS. Soil physics with BASIC-Transport models for soil-plant systems. Amsterdam: Elsevier 1994.

[14] Carrigan CR, Nitao JJ. Predictive and diagnostic simulation of in situ electrical heating in contaminated, low-permeability soils. Environ Sci Technol 2000; 34: 4835-4841.

[15] Cass A, Campbell GS, Jones TL. Enhancement of thermal water-vapor diffusion in soil. Soil Sci Soc Am J 1984; 48(1): 25-32.

[16] Cohen Y, Ryan PA. Chemical transport in the top-soil zone. The role of moisture and temperature gradients. J Hazard Mater 1989; 22(3): 283-304.

[17] de Vries DA. The theory of heat and moisture transfer in porous media revisited. Int J Heat Mass Transfer 1987; 30(7): 1343-1350.

[18] Dullien FAL. Porous media. San Diego: Academic Press, 1992.

[19] Fletcher CAJ. Computational techniques for fluid dynamics, 1. Berlin: Springler Verlag, 1991.

[20] Garnier P, Néel C, Mary B, Lafolie F. Evaluation of a nitrogen transport and transformation model in a bare soil. Eur J Soil Sci 2001; 52: 253-268.

[21] Gastó JM, Modelització i simulació numérica del transport no isotèrmic de l'aigua i de compostos orgànics volàtils en la zona no saturada del sòl, Ph. D. thesis, University Rovira i Virgili (Tarragona), Spain, 2002.

[22] Grant SA, Salehzadeh A. Calculation of temperature effects on wetting coefficients of porous solids and their capillary pressure functions. Water Resour Res 1996; 32: 261-270.

[23] Grifoll J, Cohen Y. A front-tracking numerical algorithm for liquid infiltration into nearly dry soils. Water Resour Res 1999; 35: 2579-2585.

[24] Grifoll J, Cohen Y. Chemical volatilization from the soil matrix: Transport through the air and water phases. J Hazard Mater 1994; 37: 445-457.

[25] Grifoll J, Cohen Y. Contaminant migration in the unsaturated soil zone: the effect of rainfall and evapotranspiration. J Contam Hydrol 1996; 23: 186-211.

[26] Guedes de Carvalho JRF, Delgado JMPQ. Overall map and correlation of dispersion data for flow through granular packed beds. Chem Eng Sci 2005, 60: 365-375.

[27] Haga D, Niibori Y, Chida T. Hydrodinamic dispersion and mass transfer in unsaturated flow. Water Resour Res 1999; 35(4): 1065-1077.

[28] Haridasan M, Jensen RD. Effect of temperature on pressure head-water content relationship and conductivity of two soils. Soil Sci Soc Amer Proc 1972; 36: 703-708.

[29] Haverkamp R, Vauclin M, Touma J, Wierenga PJ, Vachaud G. A comparison of numerical simulation models for one-dimensional infiltration. Soil Sci Soc Amer J 1977; 41: 286-294.

[30] Hillel D. Fundamentals of Soil Physics. San Diego: Academic Press, 1980.

[31] Hopmans JW, Dane JH. Temperature dependence of soil hydraulic properties. Soil Sci Soc Am J 1986; 50: 4-9.

[32] Hopmans JW, Dane JH. Temperature dependence of soil water retention curves. Soil Sci Soc Am J 1986; 50: 562-567.

[33] Idso SB, Aase JK, Jackson RD. Net radiation - Soil heat flux relations as influenced by soil water content variations. Bound Layer Meteor 1975; 9: 113-122.

[34] Idso SB. A set of equations for full spectrum and 8 to 14 μm and 10.5 to 12.5μm thermal radiation from cloudless skies. Water Resour Res 1981; 17: 295-304.

[35] Jackson RD. Diurnal Changes in soil water content during drying. A R.R. Bruce et al. (Editors) Field soil water regime. Special Pub. 5., Soil Sci Soc Amer Proc 1973; 37-55.

[36] Jansson PE. Simulation model for soil water and heat conditions: description of the SOIL model. Rep. 165, 72 pp., Swedish Univ of Agric Sci Div of Hydrotech, Uppsala, SW, 1991.

[37] Jin Y, Jury A. Characterizing the dependence of gas diffusion coefficient on soil properties. Soil Sci Soc Am J 1996, 60: 66-71.

[38] Judge J, Abriola LM, England AW. Numerical validation of the land surface process component of an LSP/R model. Adv Water Resour 2003; 26: 733-746.

[39] Lide DR. (Ed). Handbook of Chemistry and Physics. Boca Raton: CRC Press, 2001.

[40] Liu HH, Dane JH, Reconciliation between measured and theoretical temperature effects on soil water retention curves. Soil Sci Soc Am J 1993; 57: 1202-1207.

[41] Maciejewski S. Numerical and experimental study of solute transport in unsaturated soils. J Contam Hydrol 1993; 14: 193-206.

[42] Millington RJ, Quirk JP. Transport in porous media. In A F.A. van Beren et al. (Editors), Trans Int Congr Soil Sci. Amsterdam: Elsevier; 1960. p. 97-107.

[43] Millington RJ. Gas diffusion in porous media. Science 1959, 130: 100-102.

[44] Milly PCD. A simulation analysis of thermal effects on evaporation from soil. Water Resour Res 1984; 20(8): 1087-1098.

[45] Milly PCD. Moisture and heat transport in hysteretic, inhomogeneous porous media: A matric head-based formulation and a numerical model. Water Resour Res 1982; 18(3): 489-498.

[46] Monji N, Hamotami K, Omoto Y. Dynamic behavior of the moisture near the soil-atmosphere boundary. Bull. Univ Osaka 1990, 42: 61-69.

[47] Nassar IN, Horton R. Simultaneous transfer of heat, water, and solute in porous media: I. Theoretical development, Soil Sci Soc Am. J 1992, 56:1350-1356.

[48] Nassar IN, Horton R, Globus AM. Simultaneous transfer of heat, water, and solute in porous media: II. Experiment and analysis, Soil Sci Soc Am. J 1992, 56:1357-1365.

[49] Nassar IN, Horton R. Heat, water, and solute transfer in unsaturated porous media: I – Theory development and transport coefficient evaluation, Transport Porous Med. 1997, 27:17-38.

[50] Nassar IN, Shafey HM, Horton R. Heat, water, and solute transfer in unsaturated porous media: II –Compacted soil beneath plastic cover, Transport Porous Med. 1997, 27:39-55.

[51] Nassar IN, Globus, AM, Horton R. Simultaneous soil heat and water transfer, Soil Sci. 1992, 154:465-472.

[52] Niemi A, Kling T, Kangas M, Ettala M. Heat transport in unsaturated zone thermal energy storage – Analysis with two-phase and single-phase models. Transport Porous Med 2003; 51: 67-88.

[53] Nützmann G, Maciejewski S, Joswig K. Estimation of water saturation dependence of dispersion in unsaturated porous media: experiments and modelling analysis. Adv Water Resour 2002; 25: 565-576.

[54] Or D, Wraith JM. Comment on "On water vapor transport in field soils". Water Resour Res 2000; 36: 3103-3105.

[55] Ouyang Y, Zheng C. Surficial processes and $CO_2$ flux in soil ecosystem. J Hydrol 2000; 234: 54-70.

[56] Ouyang Y. Phytoremediation: modeling plant uptake and contaminant transport in the soil-plant atmosphere continuum. J Hydrol 2002; 266: 66-82.

[57] Parlange MB, Cahill AT, Nielsen DR, Hopmans JW, Wendroth O. Review of heat and water movement in filed soils. Soil & Tillage Research 1998, 47: 5-10.

[58] Patankar SV. Numerical heat transfer and fluid flow. New York: McGraw-Hill, 1980.

[59] Philip JR, de Vries DA. Moisture movement in porous media under temperature gradients. Transactions American Geophysical Union 1957, 38(2): 222-231.

[60] Poling BE, Prausnitz JM, O'Connell JP. The properties of gases and liquids. New York :McGraw-Hill, 2001.

[61] Press WH, Flannery BP, Teukolsky SA, Vetterling WT. Numerical recipes, Cambridge: Cambridge University Press, 1990.

[62] Rose CW. Water transport in soil with a daily temperature wave. I Theory and experiment, Aust J Soil Res 1968; 6: 31-44.

[63] Rose CW. Water transport in soil with a daily temperature wave. II Analysis, Aust J Soil Res 1968; 6: 45-57.

[64] Ruffner JA, Bair FE. (editors) The Weather Almanac, Detroit: Gale Research Co., 1987.

[65] Sahimi M, Heiba AA, Davis HT, Scriven LE. Dispersion in flow through porous media- II. Two-phase flow. Chem. Engng Sci 1986; 41(8): 2123-2136.

[66] Saravanapavan T, Salvucci GD. Analysis of rate-limiting processes in soil evaporation with implications for soil resistance models. Adv Water Res 2000; 23: 493-502.

[67] Scanlon BR, Keese K, Reedy RC, Simunek J, Andraski BJ. Variations in flow and transport in thick desert vadose zones in response to paleoclimatic forcing (0-90 kyr): Field measurements, modeling, and uncertainities. Water Resour Res 2003; 39(7): 1179, doi: 10.1029/2002WR001604.

[68] She HY, Sleep BE. The effect of temperature on capillary pressure-saturation relationships for air-water and percholoroethylene-water systems. Water Resour Res 1998; 34: 2587-2597.

[69] Simunek J, Sejna M, van Genuchten MT. The HYDRUS-1D software package for simulating the one-dimensional movement of water, heat, and multiple solutes in variably-saturated media. version 2.0, IGWMC – TPS – 70, 202 pp., Int. Groundwater Model. Cent. Colo. Sch. Of Mines, Golden, Colo., 1998.

[70] Thomas HR, He Y. Analysis of coupled heat, moisture, and air transfer in a deformable unsaturated soil. Geotechnique 1995; 45(4): 677-689.

[71] Thomson NR, Sykes, JF Van Vliet, D.. A numerical investigation into factors affecting gas and aqueous phase plumes in the subsurface. J Contam Hydrol 1997; 28: 39-70.

[72] Wescot DW, Wierenga PJ. Transfer of heat by conduction and vapor movement in a closed soil system. Soil Sci Soc Am Proc 1974, 38: 9-14.

[73] Yamanaka T, Takeda A, Shimada J. Evaporation beneath the soil surface: some observational evidence and numerical experiments. Hydrol. Process 1998; 12:2193-2203.

## LIST OF TABLES



## LIST OF FIGURES

**Table 1**. Temperature dependence of physicochemical properties of water[(a)]

| Property | Relationship |
|---|---|
| Density (kg/m$^3$)[b] | $\rho_L = 658.2 + 2.509\,T - 4.606 \cdot 10^{-3}\,T^2$ |
| Dynamic viscosity (Pa s)[b] | $\ln \mu_L = -6.434 - \frac{2414.}{T} + \frac{667300}{T^2}$ |
| Surface tension (N/m)[c] | $\sigma = 0.117 - 0.000153\,T$ |
| Vapor diffusion coefficient in air (m$^2$/s)[d] | $D_G = 2.92 \cdot 10^{-5} \left( \frac{T}{313\ K} \right)^{2.0}$ |

[a] T – temperature (K)

[b] Regression of data from Handbook of Chemistry and Physics [39] for 273 K ≤ T ≤ 333 K.

[c] From Grant and Salehzadeh [22]

[d] From Poling et al. [60]

**Table 2**. Hydraulic parameters for test cases I and II.

| | Experiment of | |
|---|---|---|
| Property | Rose[a] | Jackson[b] |
| $k_i$ (m$^2$) | 1.61x10$^{-12}$ | 2.02x10$^{-13}$ |
| $\lambda$ | 0.26 | 0.03 |
| $P_b$ (Pa) | -953 | -892 |
| $\theta_{LS}$ | 0.40 | 0.39 |
| $\theta_{LR}$ | n.a. | 0.005 |
| $\alpha$ (Pa) | n.a. | -310000 |
| $\beta$ | n.a. | 0.398 |

[a] Rose [62]

[b] Jackson [35]

n.a. Not applicable.

**Table 3**. Climatological and geographical data for test cases I and II.

| | **Experiment of** | |
|---|---|---|
| | **Rose**[a] | **Jackson**[b] |
| ***Longitude*** | 133º5' E | 112º1' W |
| ***Latitude*** | 23º45' S | 33º8' N |
| ***Start date (dd/mm)*** | 01/09 | 02/03 |
| $\overline{H}$ ***(%)*** | 29 | 60 |
| $\overline{T_a}$ ***(ºC)*** | 18. | 12.5 |
| $A_H$***(%)/***$A_T$ ***(ºC)*** | 7/8.7 | 20/7.5 |
| $\varphi_T$ / $\varphi_H$ ***(h)*** | 7/7 | 7/10 |
| ***roughness length at surface (m)*** | 0.01 | 0.01 |
| ***u (m/s)*** [c] | 3 | 3 |

[a] Rose [62]

[b] Jackson [35]

[c] Wind speed at 2 m height above soil surface.

**Figure 1**. Flow chart of the solution procedure for the coupled mass and energy transport equations.

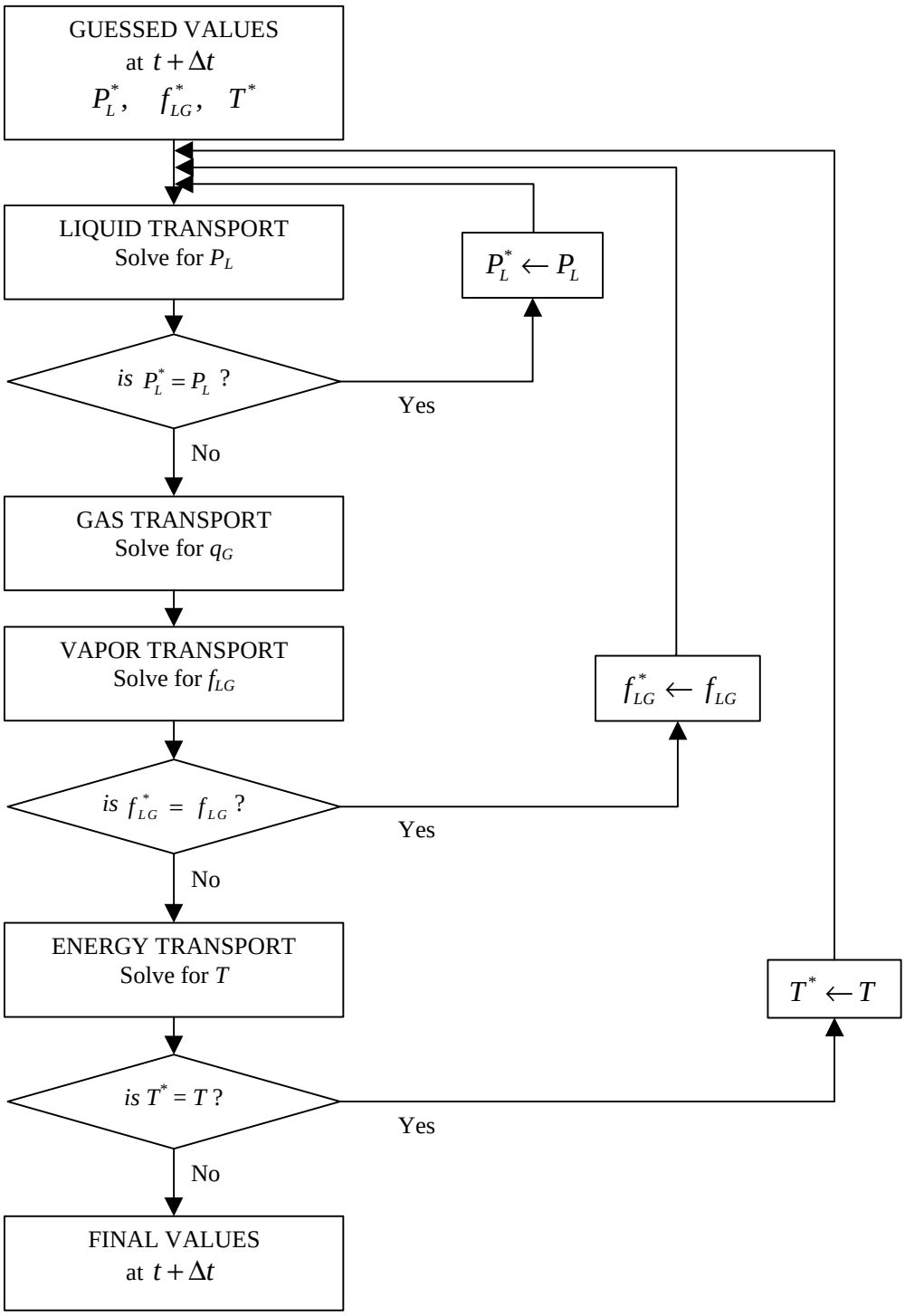

**Figure 2**. Evolution of volumetric water content during soil drying. Data points represent the gravimetric measurements of Rose (1968). Continuous lines represent moisture content at the designated depths and the dashed lines depict the integral average values between these depths.

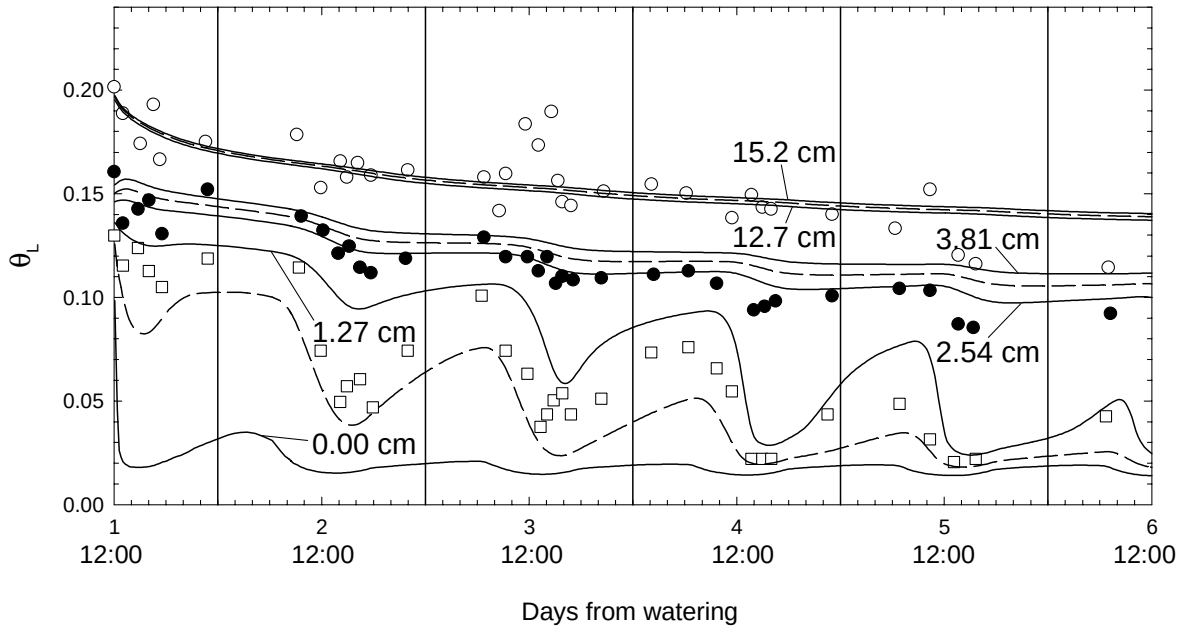

**Figure 3.** Temperature evolution at the soil surface and at depth of 13 cm. Data points are the reported measurements of Rose (1968) and solid lines are simulation results.

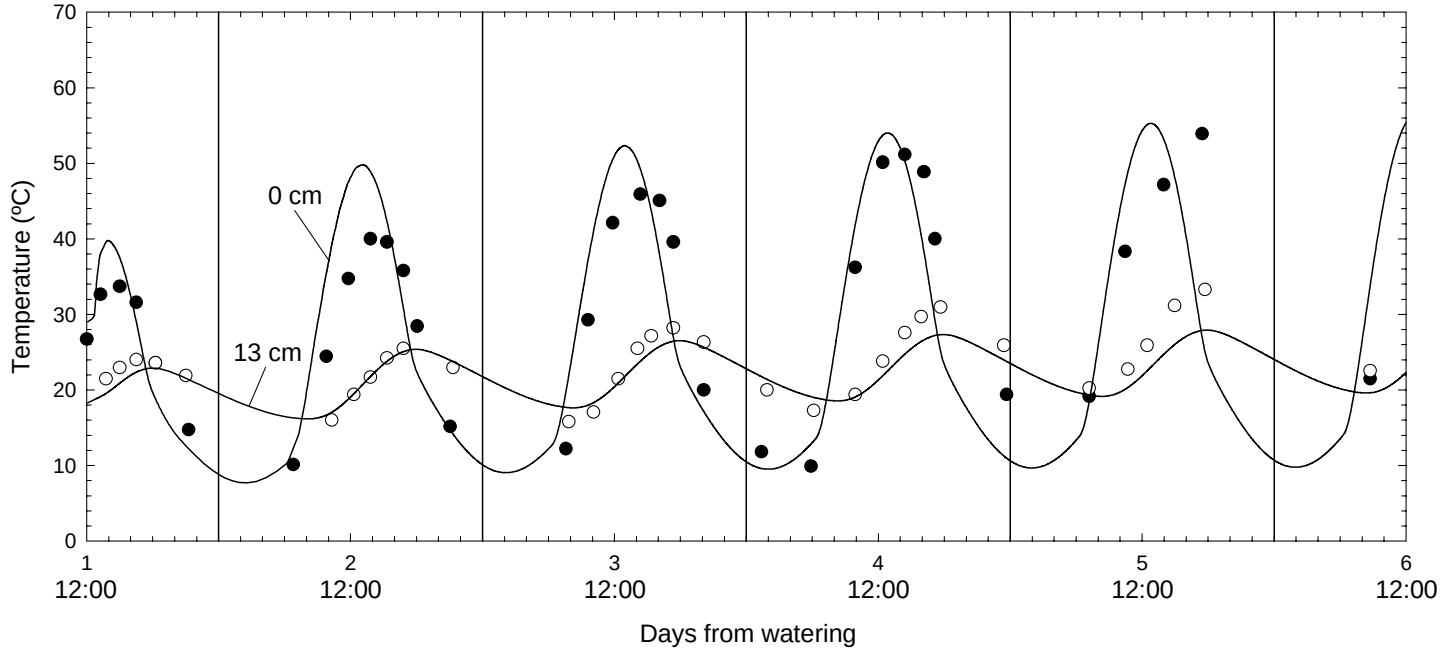

**Figure 4**. Temperature and water vapor partial pressure profiles four days after irrigation. Data points are the measurements of Rose (1968) and solid lines represent the simulation results.

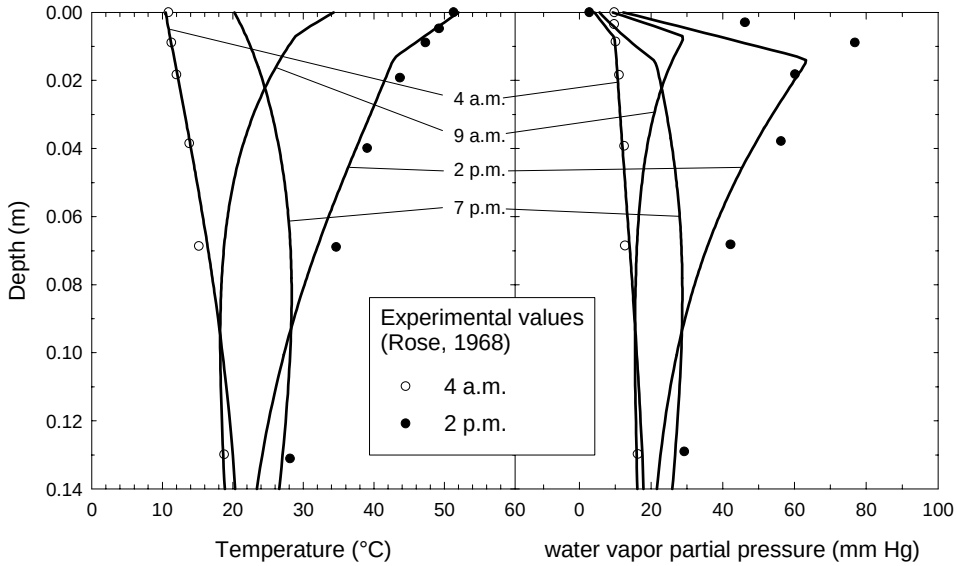


**Figure 5** Evolution of moisture content in the soil region extending from the surface to a depth of 5 mm. Data points are the measurements of Jackson (1973) and lines depict the simulation results. The dashed lines represent moisture content at the indicated depth, and the continuous solid line represent the integral average moisture content for the top soil zone (0-0.5 cm).

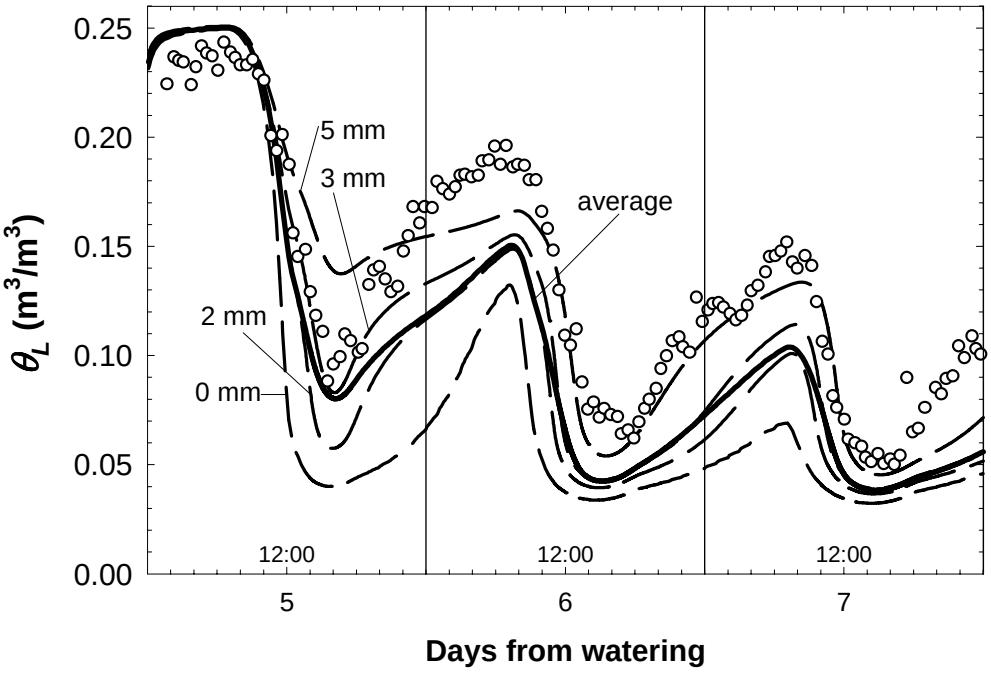

**Figure 6.** Simulations of the influence of wind speed and relative humidity on the integral average moisture content in the top soil layer (0-5 mm) for Test case II. The open symbols represent the experimental data of Jackson (1973).

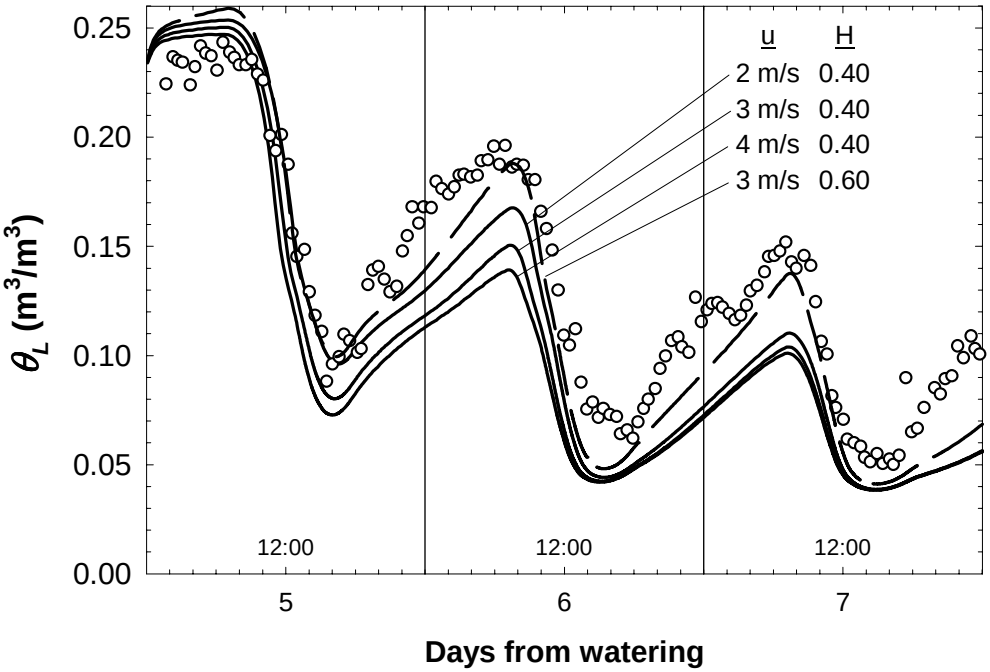


**Figure 7** Simulation profiles for water flux, moisture and temperature for the study of Jackson (1973) at 2 p.m. of day 7 after irrigation. a) Water flux profiles for each transport mechanism and b) volumetric water content and temperature profiles.